Conserved Gαq-PLCβ-PKC signaling mediates trametinib resistance in $BRAF^{V600E}$ melanoma

Jingyi Ke[1,2,3,4,5], Zi Wang[1,2,3,4,5], Zhengyang Guo[1,2,3,4,5], Guangshuo Ou[1,2,3,4,5,*], and Wei Li[6,*]

Affiliations:

[1]Tsinghua-Peking Center for Life Sciences, Tsinghua University, Beijing, China.

[2]Beijing Frontier Research Center for Biological Structure, Tsinghua University, Beijing, China.

[3]McGovern Institute for Brain Research, Tsinghua University, Beijing, China.

[4]State Key Laboratory for Membrane Biology; Beijing, China.

[5]School of Life Sciences and MOE Key Laboratory for Protein Science, Tsinghua University, Beijing, China.

[6]School of Basic Medical Sciences, Tsinghua University, Beijing, China.

*Correspondence to: guangshuoou@tsinghua.edu.cn, weili_med@mail.tsinghua.edu.cn

Abstract

Oncogenic mutations in BRAF, most commonly V600E, drive constitutive activation of the MAPK pathway in ~50% of melanomas. While MEK inhibitors such as trametinib, alone or in combination with BRAF inhibitors, are clinically effective, their therapeutic effects are restricted due to the development of drug resistance. Here we establish a *Caenorhabditis elegans* model carrying the oncogenic *lin-45(V627E)* allele, functionally equivalent to human $BRAF^{V600E}$, to investigate mechanisms of trametinib resistance. Genetic suppressor screening and transcriptomic profiling reveal that the EGL-30/Gαq-PLCβ-PKC axis promotes resistance by sustaining MAPK activity under MEK blockade. Pharmacological inhibition of PLCβ or PKC synergizes with trametinib to abolish MAPK signaling and restore drug sensitivity in worms. Importantly, this resistance mechanism is conserved in human melanoma: combined MEK and Gαq-PLCβ-PKC inhibition markedly enhances trametinib efficacy in $BRAF^{V600E}$ melanoma cells and xenografts, and reverses acquired resistance in trametinib-resistant melanoma sublines. Together, our results identify a conserved Gαq-PLCβ-PKC pathway as a driver of trametinib resistance and provide preclinical evidence for its co-targeting with MEK inhibition as a therapeutic strategy in $BRAF^{V600E}$ melanoma.

Introduction

Melanoma is the most aggressive form of skin cancer and accounts for the majority of skin cancer-related deaths worldwide (Schadendorf et al., 2018). Approximately half of melanomas harbor activating BRAF mutations, most frequently V600E, which constitutively activates the RAS-RAF-MEK-ERK (MAPK) pathway and drives tumor growth and survival (Davies et al., 2002; Halle and Johnson, 2021; Wan et al., 2004). Targeted therapies with BRAF inhibitors (BRAFi) such as vemurafenib or dabrafenib, alone or in combination with MEK inhibitors (MEKi) such as trametinib or cobimetinib, have substantially improved clinical outcomes (Adashek et al., 2022). Combined BRAFi/MEKi therapy is now the standard of care for patients with $BRAF^{V600E}$ melanoma (Dummer et al., 2018). However, responses are transient and most patients ultimately relapse due to the development of resistance, underscoring the urgent need for novel therapeutic strategies that can extend durability of MAPK pathway inhibition (Cohen and Sullivan, 2019).

Resistance to BRAFi/MEKi arises through diverse mechanisms, including MAPK pathway reactivation and engagement of compensatory signaling circuits such as MET and PI3K-AKT-mTOR (Bahar et al., 2023; Braicu et al., 2019; Kakadia et al., 2018). Despite intensive investigation, the heterogeneity and complexity of resistance networks remain incompletely understood, limiting the rational design of effective combination therapies. Evolutionarily conserved model systems that faithfully recapitulate acquired drug resistance can accelerate discovery of fundamental resistance mechanisms and uncover new therapeutic vulnerabilities.

The nematode *Caenorhabditis elegans* offers a powerful genetic model for studying conserved signaling networks. The Ras/MAPK cascade is highly conserved between *C. elegans* and humans: LIN-45, the sole worm RAF ortholog, shares 53% identity with human BRAF, while MEK-2 and MPK-1 share 52% and 81% identity with human MEK1 and ERK, respectively (Altschul et al., 1997). Importantly, the LIN-45(V627E) substitution is functionally equivalent to the oncogenic human $BRAF^{V600E}$ mutation (de la Cova and Greenwald, 2012; Han et al., 1993; Kim et al., 2018).

In *C. elegans*, the Ras-MAPK cascade affects multiple developmental and physiological processes including germline development and vulval precursor cell (VPC) fate specification (Sternberg and Han, 1998; Sundaram, 2013), offering sensitive readouts for genetic and pharmacologic perturbation. Complete loss of MAPK signaling causes sterility (Church et al., 1995; Hajnal and Berset, 2002; Hsu et al., 2002; Lackner and Kim, 1998; Lee et al., 2007; Robinson-Thiewes et al., 2021), whereas reduced signaling produces a vulvaless (Vul) phenotype and hyperactivation induces ectopic VPC induction and a multivulva (Muv) phenotype (Han and Sternberg, 1990; Lackner et al., 1994; Saffer et al., 2011; Wu et al., 1995). Misregulated MAPK signaling can also yield a protruding vulva (Pvl) due to defects in vulval lineages or the vulval–uterine connection (Cordeddu et al., 2009; Eisenmann and Kim, 2000; Flex et al., 2014). Importantly, Muv phenotypes caused by MAPK pathway hyperactivation can be suppressed by targeted inhibitors, while pharmacologic inhibition of MAPK activity in wild-type animals produces a Vul phenotype, and together these tractable and quantifiable responses have established *C. elegans* as a powerful in vivo platform for high-throughput screening of MAPK pathway inhibitors (Bae et al., 2012; Gorgoń et al., 2024; Hara and Han, 1995; Ji et al., 2019).

Here, we introduce *lin-45(V627E)* mutant worms as a tractable genetic platform for modeling trametinib resistance. Using unbiased transcriptomic profiling and genetic suppressor screens, we identify the EGL-30/Gαq-PLCβ-PKC axis as a conserved mediator of MEK inhibitor resistance. We further demonstrate this pathway promotes resistance not only in worms but also in $BRAF^{V600E}$ melanoma cells and xenografts, and that pharmacological blockade of Gαq-PLCβ-PKC signaling restores trametinib sensitivity. Our findings reveal a conserved resistance mechanism and provide a rationale for combined MEK and PLCβ/PKC inhibition as a therapeutic strategy for $BRAF^{V600E}$ melanoma.

Results

A *lin-45(V627E) C. elegans* Model Reveals Acquired Trametinib Resistance.

To establish a *C. elegans* model that recapitulates the acquired trametinib resistance observed in $BRAF^{V600E}$-driven tumors, we exposed day 1 adult wild-type (WT) and *lin-45(V627E)* mutant hermaphrodites (P0 generation) to the FDA-approved MEK inhibitor trametinib at concentrations ranging from 1 to 100 μM (Fig. 1A). As previously reported, all *lin-45(V627E)* hermaphrodites (n = 300) display Pvl phenotype (Fig. 1C) (Wang et al., 2024). In WT animals, 1 μM trametinib induced a vulvaless (Vul) phenotype in 20% of F1 progeny, and higher doses (10 μM and 100 μM) completely abolished vulval development, reflecting efficient suppression of MAPK signaling. In contrast, *lin-45(V627E)* mutants responded in a dose-dependent manner: 1 μM and 10 μM trametinib suppressed the Pvl phenotype in 100% of F1 progeny, whereas 100 μM exposure unexpectedly restored protruding vulval morphology in all mutants, a sharp contrast to the complete Vul phenotype observed in WT worms under the same condition (Fig. 1D).

To further evaluate MAPK pathway inhibition, we quantified brood sizes of F1 animals. Compared to DMSO-treated controls, WT F1 animals exposed to 1 μM trametinib showed severe brood size reduction (250 ± 49 vs. 23 ± 20, $p < 0.0001$; Fig. 1B). Complete sterility occurred in WT F1 animals treated with 10 μM or 100 μM trametinib (Fig. 1B), suggesting a complete blockade of the BRAF/MEK/ERK pathway . These observations are in line with the sterile phenotypes observed in null alleles of *lin-45*/Raf, *mek-2*/MEK, or *mpk-1*/ERK (Hsu et al., 2002; Sundaram, 2013).

DMSO-treated *lin-45(V627E)* F1 animals maintained normal brood sizes comparable to those of DMSO-treated WT animals (241 ± 59 vs. 250 ± 49, $p = 0.54$). Notably, 1 μM trametinib had no significant effect on the brood size of *lin-45(V627E)* F1 animals compared to DMSO-treated mutants (236 ± 53 vs. 241 ± 59, $p > 0.99$, Fig. 1B), suggesting that this concentration is insufficient to inhibit the constitutively active BRAF/MEK/ERK signaling in the mutant background. In contrast, treatment with 10 μM trametinib nearly abolished fertility in *lin-45(V627E)* F1 animals (4 ± 7 vs. 241 ± 59, $p < 0.0001$; Fig. 1B), indicating effective pathway suppression at this concentration. Strikingly, increasing the dose to 100 μM paradoxically restored brood size to ~63% of DMSO-treated mutant levels (153 ± 61 vs. 241 ± 59, $p = 0.0001$; Fig. 1B), implying that *lin-45(V627E)* worms had acquired resistance to high-dose MEK inhibition.

This dose-dependent resistance phenotype likely arises through reactivation of MAPK signaling or engagement of alternative signaling pathways. This phenomenon mirrors observations in BRAF-mutant melanoma cells, which acquire trametinib resistance following prolonged exposure to escalating drug concentrations (Hartman et al., 2020; Tripathi et al., 2020). Collectively, these findings establish *lin-45(V627E)* worms as a genetically tractable in vivo model for dissecting the molecular mechanisms

underlying acquired trametinib resistance.

Transcriptome Profiling and Genetic Screening Identify EGL-30/Gαq Signaling as a Mediator of Trametinib Resistance in *C. elegans.*

To elucidate the molecular mechanisms underlying acquired trametinib resistance in *lin-45(V627E)* mutants, we performed transcriptome profiling of trametinib-sensitive and -resistant *lin-45(V627E)* mutants. Specifically, we compared F1 animals derived from *lin-45(V627E)* hermaphrodites treated with 10 μM trametinib (sensitive) and 100 μM trametinib (resistant). Principal component analysis (PCA) of RNA-seq revealed a clear separation between these two populations, indicating distinct gene expression patterns (Fig. S1A). Differential expression analysis identified 443 genes that were significantly upregulated (fold change > 2 and adjusted P-value (Padj) < 0.05) in trametinib-resistant animals (Fig. 2C). Gene Ontology (GO) enrichment analysis on these genes revealed significant upregulation of genes associated with G-protein signaling pathway, including the *egl-30* gene, which encodes the *C. elegans* Gαq subunit orthologous to human GNAQ/GNA11, within the heterotrimeric G-protein complex (fold change = 2.3, Padj = 0.008; Fig. 2C-D and S1B).

Supporting this finding, a forward genetic suppressor screen uncovered a recessive allele, *egl-30(R25C)*, which suppressed the Pvl phenotype in *lin-45(V627E)* mutants (Fig. 2A). Similar phenotypes were ovserved when we introduced other *egl-30* loss-of-function mutations into the *lin-45(V627E)* background (Fig. 2B).

To evaluate the functional role of *egl-30* in trametinib resistance, we analyzed brood sizes in *lin-45(V627E); egl-30(R25C)* double mutants. Under DMSO treatment, the double mutants exhibited a severe fertility defect (Fig. 2E), producing significantly fewer progeny than either WT (13 ± 7 vs. 250 ± 49, $p < 0.0001$) or *lin-45(V627E)* single mutants (13 ± 7 vs. 241 ± 59, $p < 0.0001$). Similar to *lin-45(V627E)* single mutants, the double mutants remained fertile at 1 μM trametinib but became sterile at 10 μM (Fig. 2E). Notably, while 100 μM trametinib partially restored fertility in *lin-45*(*V627E*) single mutants (63% of DMSO controls), this rescue was substantially impaired in the double mutants, with brood size reduced to 12% of DMSO controls (2 ± 2 vs.13 ± 7; Fig. 2E). These findings indicate that reduced EGL-30/Gαq activity compromises the resistance phenotype, supporting a critical role for Gαq signaling in mediating high-dose trametinib resistance.

EGL-30/Gαq Signaling Promotes Trametinib Resistance in *C. elegans* through Its Canonical Downstream Pathway.

To further explore how EGL-30/Gαq signaling contributes to trametinib resistance, we examined its canonical downstream signaling cascade. Gαq typically activates phospholipase Cβ (PLCβ), which hydrolyzes phosphatidylinositol 4,5-bisphosphate (PIP_2) into inositol 1,4,5-trisphosphate (IP_3) and diacylglycerol (DAG). DAG subsequently activates protein kinase C (PKC), which phosphorylates a range of downstream targets, including C-Raf, thereby initiating MAPK pathway activation

(Kolch et al., 1993). Based on this well-established signaling cascade, we hypothesized that the EGL-30/Gαq-PLCβ-PKC axis enables *lin-45(V627E)* mutants to bypass MEK inhibition and maintain MAPK activity under high-dose trametinib treatment, thereby enabling *lin-45(V627E)* worms to retain fertility.

To test this, we treated *lin-45(V627E)* adults with either the PLCβ inhibitor U73122 or the PKC inhibitor Sotrastaurin, alone or in combination with trametinib. Sotrastaurin, currently in Phase II clinical trials, demonstrates minimal off-target activity even at elevated concentrations (Klaeger et al., 2017). Treatment with 50 μM U73122 or 50 μM Sotrastaurin alone had minimal effects on fertility compared to DMSO controls (U73122: 240 ± 32 vs. 241 ± 59, $p = 0.33$; Sotrastaurin: 222 ± 40 vs. 241 ± 59, $p = 0.01$; Fig. 2F). In contrast, co-treatment with 100 μM trametinib and either inhibitor resulted in complete sterility (Fig. 2F), phenocopying the genetic suppression of *egl-30(R25C)*. Together, these findings establish the EGL-30/Gαq-PLCβ-PKC signaling axis as a critical mediator of adaptive resistance to MEK inhibition, and highlight it as a potential therapeutic target in MAPK-driven malignancies.

Combined Inhibition of Gαq-PLCβ-PKC Signaling and MEK Synergistically Suppresses Proliferation of BRAF^{V600E} Melanoma Cell Lines.

To assess whether the resistance mechanism identified in *C. elegans* is conserved in human cancer cells, we investigated whether inhibition of the Gαq-PLCβ-PKC pathway enhances the sensitivity of BRAF^{V600E} melanoma cells to MEK inhibition. We first performed shRNA-mediated knockdown of two Gαq paralogs, GNAQ and GNA11, in A375 melanoma cells harboring the BRAF^{V600E} mutation (Fig. 3C). While knockdown of GNAQ/GNA11 had minimal effect on basal proliferation (Fig. 3A), it markedly reduced the IC_{50} of trametinib in A375 cells (0.14 nM vs. 0.04 nM and 0.04 nM, $p < 0.01$; Fig. 3B). Knockdown of GNAQ/11 markedly reduced p-ERK levels, indicating that Gαq is required for ERK phosphorylation (Fig. 3D). Thus, loss of Gαq signaling potentiated trametinib sensitivity, indicating a synergistic interaction between MEK inhibition and Gαq blockade.

We next assessed pharmacological inhibition of the Gαq-PLCβ-PKC pathway in combination with trametinib. Co-treatment with trametinib and the PLCβ inhibitor U73122 or the PKC inhibitor sotrastaurin produced robust synergistic effects on A375 cell proliferation across a broad range of concentrations (Fig. 3E-F). Drug interactions were quantified using the Chou-Talalay combination index (CI) (Chou and Talalay, 1984). Notably, in most dose combinations, CI values for trametinib-U73122 and trametinib-sotrastaurin were <0.3 (Fig. 3E-F), further supporting strong synergy between MEK inhibition and suppression of the Gαq-PLCβ-PKC pathway. Consistent with these effects on proliferation, trametinib alone reduced ERK phosphorylation, while combined treatment produced a more pronounced and synergistic suppression of ERK activation (Fig. 3G). These findings in human melanoma cells parallel the genetic interactions observed in *lin-45(V627E)* nematodes, highlighting the

evolutionary conservation of this resistance mechanism.

Combining Trametinib with PLCβ/PKC Inhibitors Suppresses Tumor Growth in Vivo.

To assess the in vivo efficacy of combined MEK and PLCβ/PKC inhibition, we established A375 xenografts in nude mice. Tumors in vehicle-treated animals grew rapidly, whereas monotherapies with trametinib, U73122, or sotrastaurin significantly delayed tumor progression relative to vehicle controls. Notably, combination treatments (U73122 + trametinib and sotrastaurin + trametinib) resulted in markedly enhanced tumor suppression compared to either agent alone (Fig. 4), indicating a synergistic anti-tumor effect in vivo. Importantly, treatment with trametinib, sotrastaurin, or their combination had no discernible effect on body weight, suggesting good tolerability. In contrast, mice receiving U73122 alone or in combination with trametinib exhibited a modest but measurable reduction in body weight, indicating potential systemic effects at the tested dose (Fig. S2).

Blockade of Gαq-PLCβ-PKC Reverses Acquired Trametinib Resistance in Melanoma.

To determine whether Gαq-PLCβ-PKC activation is necessary for the maintenance of acquired trametinib resistance, we established polyclonal trametinib-resistant A375 cell lines (A375-TR) through prolonged exposure to increasing concentrations of the drug (Fig. 5A). As expected, parental A375 cells were highly sensitive to trametinib (IC_{50} = 0.5 nM), whereas A375-TR cells displayed a significantly higher IC_{50} (266 nM, $p = 0.01$, Fig. 5B). Under high concentrations of trametinib treatment, A375-TR cell line retained higher levels of phosphorylated ERK compared to the parental cells (Fig. 5C).

Knockdown of GNAQ/GNA11 significantly reduced the IC_{50} of trametinib and ERK activationin A375-TR cells (576 nM vs. 128 nM and 255 nM, $p < 0.01$; Fig. 5D-G), indicating that suppression of Gαq signaling restores drug sensitivity. Treatment of A375-TR cells with either the PLCβ inhibitor U73122 or the PKC inhibitor sotrastaurin substantially reduced cell viability (Fig. 5H-I). Notably, co-treatment with trametinib further potentiated the anti-proliferative effects of both inhibitors (Fig. 5H-I), consistent with a synergistic interaction. Across most dose combinations, the CI values for trametinib-U73122 and trametinib-sotrastaurin were <0.3 (Fig. 5H-I), confirming strong synergy. Combined treatment resulted in a marked and potent suppression of ERK activation in A375-TR cells (Fig. 5J). These findings indicate that sustained Gαq-PLCβ-PKC signaling is critical for maintaining the resistant phenotype and that pharmacological blockade of this axis can restore trametinib sensitivity in resistant melanoma cells.

Discussion

Resistance to MAPK pathway inhibitors remains a major barrier to durable responses in $BRAF^{V600E}$ melanoma. Here, we identify a conserved Gαq-PLCβ-PKC signaling axis as a critical mediator of trametinib resistance. Using a genetically tractable *C. elegans* model carrying the *lin-45(V627E)* mutation, functionally equivalent to human $BRAF^{V600E}$, we show that Gαq signaling enables adaptive MAPK reactivation under MEK inhibition. Importantly, this adaptive mechanism is conserved in human $BRAF^{V600E}$ melanoma, where pharmacological blockade of the Gαq-PLCβ-PKC axis restores trametinib sensitivity in cell lines and xenografts. These findings reveal a previously unrecognized resistance circuit and provide a translationally actionable strategy for improving the efficacy of MEK inhibition.

The cross-species conservation of this resistance mechanism highlights the power of *C. elegans* as a model for cancer drug resistance. Worms provide a rapid, whole-organism platform for genetic and pharmacologic interrogation, enabling the discovery of signaling pathways that are not easily predicted from human data alone. *C. elegans* has been successfully employed as an in vivo platform for screening inhibitors of the MAPK/ERK pathway (Bae et al., 2012; Gorgoń et al., 2024; Hara and Han, 1995; Ji et al., 2019). Our work advances this field by demonstrating that worms can also faithfully model acquired resistance to targeted therapies. Through whole-organism genetics, we uncovered the Gαq-PLCβ-PKC pathway as an unrecognized resistance mechanism, subsequently validated in human $BRAF^{V600E}$ melanoma.

Previous reports have shown that oncogenic GNAQ mutations confer intrinsic resistance to BRAF inhibition in melanoma (Maziarz et al., 2018; Turajlic et al., 2014). Our findings extend this paradigm by demonstrating that Gαq signaling also underlies acquired resistance to MEK inhibition, with the PLCβ-PKC module as the operative effector. Thus, Gαq signaling emerges as a shared mediator of both intrinsic and acquired resistance, reinforcing its clinical relevance and supporting combined MEK-PKC targeting in $BRAF^{V600E}$ melanoma.

Our data highlight the functional versatility of Gαq-PKC signaling across melanoma subtypes. In uveal melanoma, activating GNAQ/GNA11 mutations establish this pathway as a lineage-defining oncogenic driver, and combined Gαq-PKC and MEK inhibition synergistically induces potent antitumor effects (Chen et al., 2014; Hitchman et al., 2021; Ma et al., 2021). By contrast, in $BRAF^{V600E}$ cutaneous melanoma, the same pathway is co-opted as an adaptive bypass to sustain ERK signaling during MEK blockade. This convergence underscores the broad therapeutic relevance of Gαq-PKC signaling while emphasizing its context-dependent biology: driver dependence in uveal melanoma versus resistance circuitry in cutaneous melanoma.

Therapeutically, our findings provide a strong rationale for co-targeting MEK and the Gαq-PLCβ-PKC axis in $BRAF^{V600E}$ melanoma. Both genetic and pharmacologic inhibition of this pathway produced robust synergy with trametinib, suppressed ERK reactivation, and restored drug sensitivity in resistant cells. PKC inhibitors such as sotrastaurin, which are already in clinical evaluation, demonstrated particularly favorable combinatorial activity, supporting the feasibility of rapid translational development. Given the limited durability of current BRAFi/MEKi regimens, integrating Gαq-PKC blockade represents a promising avenue to overcome resistance and extend progression-free survival.

In conclusion, our work establishes a novel experimental pipeline that begins with mechanistic discovery in *C. elegans* and extends to translational validation in human melanoma. By identifying Gαq-PLCβ-PKC signaling as a conserved resistance mechanism and therapeutic target, we provide preclinical evidence for a new combination therapy strategy in $BRAF^{V600E}$ melanoma. Future studies should explore the broader applicability of this approach in other MAPK-driven malignancies.

Materials and methods

Worm strains and culture

C. elegans were maintained according to the standard methods (Brenner, 1974). All worms were cultivated at 20 °C on nematode growth medium (NGM) plates seeded with the *Escherichia coli* OP50 unless stated otherwise. ***Adult hermaphrodite*** worms were used in the live-cell imaging experiments. The wild-type strain was Bristol N2. Some strains were provided by the Caenorhabditis Genetics Center (CGC), which is funded by the NIH Office of Research Infrastructure Programs (P40 OD010440).

Forward genetic screens

We used forward genetic screens to isolate *lin-45 (V627E)* suppressors. The *lin-45 (V627E)* mutant animals (P0) were synchronized at the late L4 larval stage, collected in 4 mL M9 buffer, and incubated with 50 mM ethyl methanesulfonate (EMS) for 4 hours at room temperature with constant rotation. Animals were then washed with M9 three times and cultured under standard conditions. After 20 hours, adult animals were bleached. Eggs (F1) were distributed and raised on ~800 9-cm NGM plates, each containing 50 to 100 eggs. Adult F2 animals on each plate were screened. Mutant animals with normal vulva were individually cultured, and their progenies were further observed. We identified mutations using whole-genome sequencing and mapped *egl-30 (R25C)* on chromosome I. We confirmed gene cloning using multiple alleles and rescue experiments.

Brood Size Assay

Synchronized L4 worms or dauer-stage worms were transferred singly to NGM plates with *E. coli* OP50 bacteria cultured with Luria-Bertani broth. Worms were repeatedly transferred to a freshly seeded NGM plate every 24 h until reproduction ceased. We counted the number of progeny at their L3/L4 stages. Our measured WT brood size is consistent with the previous results. Total brood sizes were analyzed using one-way ANOVA followed by Tukey's multiple comparisons test (GraphPad Prism 10). Data are presented as mean ± SEM, and $p < 0.05$ was considered statistically significant. Each data point represents an individual worm, with experiments repeated independently at least three times.

Genome editing

CRISPR-Cas9 constructs were purified with AxyPrep Plasmid Purification Miniprep Kit (Axygen, #AP-MN-P-250) and PureLink Quick PCR purification Kit (Invitrogen, #K310001) and co-injected into the gonads of young adult worms with the *rol-6 (su1006)* selection marker. F1 transgenic progenies were singled and screened by PCR. All variations and deletions were verified by the Sanger sequencing of the entire genes, and no other mutations were inserted on the target genes.

Microinjection and transgenic strains

For transgenic *C. elegans* experiments, transgenic lines were generated by injecting the DNA constructs into the gonads of the indicated worm strains. The co-injected selection marker was *rol-6(su1006)*. At least two independent transgenic lines with the constant transmission rate (>50%) were propagated. Concentrations of DNA constructs used for generating knock-in were 50 ng/μl, and for overexpression was 20 ng/μl.

Cell culture and treatment

The human melanoma cell line A375 was a gift from Prof. Jiang Peng (Tsinghua University) and was cultured in DMEM (Gibco) containing 10 % fetal bovine serum (Gibco) and 1 % penicillin and streptomycin (Yeasen) at 37 ℃ with 5 % CO2. A375-TR (A375-trametinib resistant) cell lines were established from A375 cells by chronic treatment with gradually increasing concentrations of trametinib and were selected for monoclones using the limiting dilution method.

Short hairpin RNA (shRNA) constructs targeting human GNA11 and GNAQ were designed and generated via molecular cloning. Two target sequences were used: shRNA#1, 5′-CCGGAGCTCAAGCTGCTGCTGCTCGCTCGAGCGAGCAGCAGCAGCTTGAGCTTTTTTG-3′, and shRNA#2, 5′-CCGGACCCCTGGTTCCAGAACTCCTCTCGAGAGGAGTTCTGGAACCAGGGGTTTTTTG-3′. A non-targeting control shRNA was purchased from Thermo Fisher Scientific. Lentiviral particles were produced and used to infect A375 and A375-TR melanoma cells. Stable cell lines expressing shRNA were selected according to the manufacturer's instructions using puromycin and maintained under selection for downstream experiments.

Cell viability assays and combination index calculation

The Cell-ATP Viability Detection Kit (HY-K0302; MedChemExpress) was adopted to determine the Cell viability of each group. Cells were incubated with serial dilutions of drugs alone or two-drug combinations in complete culture medium for 72 h. At least three independent experiments were performed. The curve-fitting software, GraphPad Prism version 10 (GraphPad Software, SanDiego, CA, USA), was used to calculate half-maximal inhibitory concentration values. Combination index (CI) values were calculated using the Chou-Talalay method implemented in the synergy Python package (Wooten and Albert, 2021).

Clonogenic assay

Cells were seeded in six-well plates at low density (100 cells/well) and cultured with drugs for 10 days, after which colonies were fixed with methanol and stained with 1× crystal violet. The quantification of the number of colonies and average colony area were analysed by using ImageJ.

Mouse xenografts and in vivo drug studies

All animal experiments were approved by the Animal Care and Use Committee at Tsinghua University. BALB/c-nude mice were housed in a temperature-controlled environment at around 21 °C with a 12 hr light/12 hr dark cycle and free access to food and water. 5×10^6 A375 $BRAF^{V600E}$ melanoma cells were resuspended in PBS were injected subcutaneously into the flanks of 5-week-old immunodeficient BALB/C-nude female mice (at least 6 mice per group). Tumor formation was monitored twice a week, and tumor volume based on calliper measurements was calculated by the modified ellipsoidal formula (tumor volume = $1/2(\text{length} \times \text{width}^2)$). When tumors reached a volume of approximately 250 mm^3, mice were randomized into four treatment arms: no drug, MEK inhibitor trametinib only, PLCβ inhibitor U73122/PKC inhibitor sotrastaurin only or the combination of trametinib and U73122/sotrastaurin. 100 mg/kg Sotrastaurin (#HY-10343, MCE) or 0.2 mg/kg trametinib (#C16249920, MACKLIN) were formulated in a vehicle consisting of 5% DMSO (#196055, MP Biomedicals), 40% PEG300 (#HY-Y0873, MCE), 5% Tween-80 (#HY-Y1891, MCE), and 50% sterile saline solution (v/v). Drugs were dissolved in this vehicle and administered via oral gavage at a volume of 100 μL per mouse. Treatment was performed three times per week. 50 mg/kg U73122 (#HY-13419, MCE) was ground into a fine powder and suspended in sterile saline to prepare a homogeneous suspension. Mice received 100 μL of the suspension via intraperitoneal injection. Treatment was performed three times per week. Control animals received either the vehicle solution or sterile saline alone, following the same route and dosing schedule as the corresponding treatment groups.

Western Blot Analysis

Cells were washed three times with cold phosphate-buffered saline (PBS) to remove residual medium and debris. After washing, cells were lysed using RIPA lysis buffer (#C0121, Beyotime) supplemented with complete protease inhibitors and phosSTOP phosphatase inhibitors (Roche). Lysates were clarified by centrifugation at 14,000 × g for 15 minutes at 4 °C to remove insoluble debris. The supernatants were collected and stored at -80 °C until further analysis.

5× SDS loading buffer (#20315ES20, Yeasen) and boiled for 5 min at 95 °C for Western blotting. Proteins were separated by FastPAGE precast gel (#TSP024-15, TSINGKE) electrophoresis and transferred to a polyvinylidene fluoride membrane (#B36011, ESAYBIO). The membrane was blocked by 5% BSA and incubated overnight with the primary antibodies at 4 °C. After washing with 10× TBST buffer containing 5‰ Tween 20 (#T1081, Solarbio) three times, the membrane was incubated with the secondary antibodies for 1 h on a shaker. Protein bands were visualized by chemiluminescence using the SuperSignal West Dura (Thermo Fisher Scientific, 34076).

The following antibodies were used: alpha-Tubulin (DM1A) Mouse mAb (#3873T, CST), anti-mouse IgG HRP-linked Antibody (#7076P2, CST), anti-rabbit IgG, HRP-linked antibody (#7074P2 ,CST), Galpha(q) (D5V1B) rabbit mAb (#14373S

, CST), p44/42 MAPK (Erk1/2) (137F5) Rabbit mAb (#4695T, CST), Phospho-p44/42 MAPK (Erk1/2) (Thr202/Tyr204) (D13.14.4E) XP Rabbit mAb (#4370T, CST).

RNA sequencing

Synchronized worms were cultured on NGM plates with the OP50 bacteria. Day 1 adult worms were harvested 24 hours after the fourth larval (L4) stage and then lysed with TRIzol reagent (Invitrogen). For cell lines, after treatment with serial dilutions of drugs alone or two-drug combinations in complete culture medium for 24 h, A375 or A375-TR cells were lysed with TRIzol reagent (Invitrogen). Total RNA was extracted according to the manufacturer's protocol. SUPERase•InTM RNase Inhibitor (Invitrogen) was used in each step to prevent RNA from degradation. RNA concentration was quantified using the Qubit RNA High Sensitivity Assay Kit (Invitrogen). RNA quality was assessed with the Agilent 2100 bioanalyzer system, and samples with an RNA integrity number (RIN) above 6.0 were used to construct the library, 50 ng to 500 ng of total RNA was used for library preparation using the KAPA RNA HyperPrep Kit (KAPA Biosystems). Library samples were analyzed by Agilent 2100 bioanalyzer system and Qubit for quality control and quantification. The samples were sequenced on an Illumina HiSeq platform. A total of 150-bp paired-end reads were generated.

Molecular biology

We followed the established protocols to perform the genome editing experiments in *C. elegans* (Dickinson et al., 2013; Friedland et al., 2013). We used the CRISPR design tool (https://zlab.bio/guide-design-resources) to select the target sequence. The sgRNA sequences were inserted to the pDD162 vector (Addgene #47549) by linearizing this vector with 15 bp overlapped primers. The resulting PCR products containing 15 bp overlapped double-strand DNA ends were treated with DpnI (NEB, #R0176V) digestion 4 hours and transformed into *E. coli*. The linearized PCR products were cyclized to generate plasmids by spontaneous recombination in bacteria.

Short hairpin RNAs (shRNAs) targeting *GNA11* and *GNAQ* were designed based on published sequences. Oligonucleotides encoding the hairpin sequences were synthesized, annealed, and cloned into the vector pLKO.1 plasmid downstream of the U6 promoter via standard molecular cloning techniques following standard protocols. Ligated products were transformed into E. coli DH5α, and positive clones were confirmed by colony PCR and Sanger sequencing.

Imaging

Adult *C. elegans* hermaphrodites were anesthetized using 1 μM levamisole in M9 buffer, mounted on 3% agarose pads, maintained at room temperature and imaged immediately. A Zeiss LSM900 confocal microscope equipped with a 100×/1.46 oil

objective and controlled by ZEN software (Carl Zeiss) was utilized. All images were acquired using a Zeiss Axio Observer (bright-field mode).

Acknowledgements
This work was supported by the National Key R&D Program of China Grants 2022YFA1302700，2024YFA1307301; and National Natural Science Foundation of China Grants 32270773 (W.L.), 32470730 (W.L.),992254306 (G.O.), 32430026 (G.O.), 32021002 (G.O.) and 31991191 (G.O.).

Competing interests: G.O., W.L., J.K., and Z.W. are inventors on patent application no. CN202511508363.0, submitted by Tsinghua University, which covers the combined use of MEK inhibitors and PLCβ/PKC signaling pathway inhibitors and their application in the treatment of $BRAF^{V600E}$ mutant tumors.

References

Adashek, J.J., A.K. Menta, N.K. Reddy, A.P. Desai, J. Roszik, and V. Subbiah. 2022. Tissue-Agnostic Activity of BRAF plus MEK Inhibitor in BRAF V600-Mutant Tumors. *Mol Cancer Ther*. 21:871-878.

Altschul, S.F., T.L. Madden, A.A. Schäffer, J. Zhang, Z. Zhang, W. Miller, and D.J. Lipman. 1997. Gapped BLAST and PSI-BLAST: a new generation of protein database search programs. *Nucleic Acids Res*. 25:3389-3402.

Bae, Y.K., J.Y. Sung, Y.N. Kim, S. Kim, K.M. Hong, H.T. Kim, M.S. Choi, J.Y. Kwon, and J. Shim. 2012. An in vivo C. elegans model system for screening EGFR-inhibiting anti-cancer drugs. *PLoS One*. 7:e42441.

Bahar, M.E., H.J. Kim, and D.R. Kim. 2023. Targeting the RAS/RAF/MAPK pathway for cancer therapy: from mechanism to clinical studies. *Signal Transduction and Targeted Therapy*. 8:455.

Braicu, C., M. Buse, C. Busuioc, R. Drula, D. Gulei, L. Raduly, A. Rusu, A. Irimie, A.G. Atanasov, O. Slaby, C. Ionescu, and I. Berindan-Neagoe. 2019. A Comprehensive Review on MAPK: A Promising Therapeutic Target in Cancer. *Cancers (Basel)*. 11.

Brenner, S. 1974. The genetics of Caenorhabditis elegans. *Genetics*. 77:71-94.

Chen, X., Q. Wu, L. Tan, D. Porter, M.J. Jager, C. Emery, and B.C. Bastian. 2014. Combined PKC and MEK inhibition in uveal melanoma with GNAQ and GNA11 mutations. *Oncogene*. 33:4724-4734.

Chou, T.C., and P. Talalay. 1984. Quantitative analysis of dose-effect relationships: the combined effects of multiple drugs or enzyme inhibitors. *Adv Enzyme Regul*. 22:27-55.

Church, D.L., K.L. Guan, and E.J. Lambie. 1995. Three genes of the MAP kinase cascade, mek-2, mpk-1/sur-1 and let-60 ras, are required for meiotic cell cycle progression in Caenorhabditis elegans. *Development*. 121:2525-2535.

Cohen, J.V., and R.J. Sullivan. 2019. Developments in the Space of New MAPK Pathway Inhibitors for BRAF-Mutant Melanoma. *Clin Cancer Res*. 25:5735-5742.

Cordeddu, V., E. Di Schiavi, L.A. Pennacchio, A. Ma'ayan, A. Sarkozy, V. Fodale, S. Cecchetti, A. Cardinale, J. Martin, W. Schackwitz, A. Lipzen, G. Zampino, L. Mazzanti, M.C. Digilio, S. Martinelli, E. Flex, F. Lepri, D. Bartholdi, K. Kutsche, G.B. Ferrero, C. Anichini, A. Selicorni, C. Rossi, R. Tenconi, M. Zenker, D. Merlo, B. Dallapiccola, R. Iyengar, P. Bazzicalupo, B.D. Gelb, and M. Tartaglia. 2009. Mutation of SHOC2 promotes aberrant protein N-myristoylation and causes Noonan-like syndrome with loose anagen hair. *Nat Genet*. 41:1022-1026.

Davies, H., G.R. Bignell, C. Cox, P. Stephens, S. Edkins, S. Clegg, J. Teague, H. Woffendin, M.J. Garnett, W. Bottomley, N. Davis, E. Dicks, R. Ewing, Y. Floyd, K. Gray, S. Hall, R. Hawes, J. Hughes, V. Kosmidou, A. Menzies, C. Mould, A. Parker, C. Stevens, S. Watt, S. Hooper, R. Wilson, H. Jayatilake, B.A. Gusterson, C. Cooper, J. Shipley, D. Hargrave, K. Pritchard-Jones, N. Maitland, G. Chenevix-Trench, G.J. Riggins, D.D. Bigner, G. Palmieri, A. Cossu, A. Flanagan, A. Nicholson, J.W. Ho, S.Y. Leung, S.T. Yuen, B.L. Weber, H.F. Seigler, T.L. Darrow, H. Paterson, R. Marais, C.J. Marshall, R. Wooster, M.R. Stratton, and P.A. Futreal. 2002. Mutations of the BRAF gene in human cancer. *Nature*. 417:949-954.

de la Cova, C., and I. Greenwald. 2012. SEL-10/Fbw7-dependent negative feedback regulation of LIN-45/Braf signaling in C. elegans via a conserved phosphodegron. *Genes Dev*. 26:2524-2535.

Dickinson, D.J., J.D. Ward, D.J. Reiner, and B. Goldstein. 2013. Engineering the Caenorhabditis elegans genome using Cas9-triggered homologous recombination. *Nat Methods*. 10:1028-1034.

Dummer, R., P.A. Ascierto, H.J. Gogas, A. Arance, M. Mandala, G. Liszkay, C. Garbe, D. Schadendorf, I. Krajsova, R. Gutzmer, V. Chiarion-Sileni, C. Dutriaux, J.W.B. de Groot, N. Yamazaki, C. Loquai, L.A. Moutouh-de Parseval, M.D. Pickard, V. Sandor, C. Robert, and K.T. Flaherty. 2018. Encorafenib plus binimetinib versus vemurafenib or encorafenib in patients with BRAF-mutant melanoma (COLUMBUS): a multicentre, open-label, randomised phase 3 trial. *Lancet Oncol*. 19:603-615.

Eisenmann, D.M., and S.K. Kim. 2000. Protruding vulva mutants identify novel loci and Wnt signaling factors that function during Caenorhabditis elegans vulva development. *Genetics*. 156:1097-1116.

Flex, E., M. Jaiswal, F. Pantaleoni, S. Martinelli, M. Strullu, E.K. Fansa, A. Caye, A. De Luca, F. Lepri, R. Dvorsky, L. Pannone, S. Paolacci, S.C. Zhang, V. Fodale, G. Bocchinfuso, C. Rossi, E.M. Burkitt-Wright, A. Farrotti, E. Stellacci, S. Cecchetti, R. Ferese, L. Bottero, S. Castro, O. Fenneteau, B. Brethon, M. Sanchez, A.E. Roberts, H.G. Yntema, I. Van Der Burgt, P. Cianci, M.L. Bondeson, M. Cristina Digilio, G. Zampino, B. Kerr, Y. Aoki, M.L. Loh, A. Palleschi, E. Di Schiavi, A. Care, A. Selicorni, B. Dallapiccola, I.C. Cirstea, L. Stella, M. Zenker, B.D. Gelb, H. Cave, M.R. Ahmadian, and M. Tartaglia. 2014. Activating mutations in RRAS underlie a phenotype within the RASopathy spectrum and contribute to leukaemogenesis. *Hum Mol Genet*. 23:4315-4327.

Friedland, A.E., Y.B. Tzur, K.M. Esvelt, M.P. Colaiacovo, G.M. Church, and J.A. Calarco. 2013. Heritable genome editing in C. elegans via a CRISPR-Cas9 system. *Nat Methods*. 10:741-743.

Gorgoń, S., O. Billing, A.U. Eriksson, and O. Hemmingsson. 2024. A Drug Discovery Pipeline for MAPK/ERK Pathway Inhibitors in Caenorhabditis elegans. *Cancer Res Commun*. 4:2454-2462.

Hajnal, A., and T. Berset. 2002. The C.elegans MAPK phosphatase LIP-1 is required for the G(2)/M meiotic arrest of developing oocytes. *Embo j*. 21:4317-4326.

Halle, B.R., and D.B. Johnson. 2021. Defining and Targeting BRAF Mutations in Solid Tumors. *Curr Treat Options Oncol*. 22:30.

Han, M., A. Golden, Y. Han, and P.W. Sternberg. 1993. C. elegans lin-45 raf gene participates in let-60 ras-stimulated vulval differentiation. *Nature*. 363:133-140.

Han, M., and P.W. Sternberg. 1990. let-60, a gene that specifies cell fates during C. elegans vulval induction, encodes a ras protein. *Cell*. 63:921-931.

Hara, M., and M. Han. 1995. Ras farnesyltransferase inhibitors suppress the phenotype resulting from an activated ras mutation in Caenorhabditis elegans. *Proc Natl Acad Sci U S A*. 92:3333-3337.

Hartman, M.L., M. Sztiller-Sikorska, A. Gajos-Michniewicz, and M. Czyz. 2020. Dissecting Mechanisms of Melanoma Resistance to BRAF and MEK Inhibitors Revealed Genetic and Non-Genetic Patient- and Drug-Specific Alterations and Remarkable Phenotypic Plasticity. *Cells*. 9.

Hitchman, T.D., G. Bayshtok, E. Ceraudo, A.R. Moore, C. Lee, R. Jia, N. Wang, M.R. Pachai, A.N. Shoushtari, J.H. Francis, Y. Guan, J. Chen, M.T. Chang, B.S. Taylor, T.P. Sakmar, T. Huber, P. Chi, and Y. Chen. 2021. Combined Inhibition of Gα(q) and MEK Enhances Therapeutic Efficacy in Uveal Melanoma. *Clin Cancer Res*. 27:1476-1490.

Hsu, V., C.L. Zobel, E.J. Lambie, T. Schedl, and K. Kornfeld. 2002. Caenorhabditis elegans lin-45 raf is essential for larval viability, fertility and the induction of vulval cell fates. *Genetics*. 160:481-492.

Ji, J., J. Yuan, X. Guo, R. Ji, Q. Quan, M. Ding, X. Li, and Y. Liu. 2019. Harmine suppresses hyper-activated Ras-MAPK pathway by selectively targeting oncogenic mutated Ras/Raf in Caenorhabditis elegans. *Cancer Cell Int*. 19:159.

Kakadia, S., N. Yarlagadda, R. Awad, M. Kundranda, J. Niu, B. Naraev, L. Mina, T. Dragovich, M. Gimbel, and F. Mahmoud. 2018. Mechanisms of resistance to BRAF and MEK inhibitors and clinical update of US Food and Drug Administration-approved targeted therapy in advanced melanoma. *Onco Targets Ther*. 11:7095-7107.

Kim, W., R.S. Underwood, I. Greenwald, and D.D. Shaye. 2018. OrthoList 2: A New Comparative Genomic Analysis of Human and Caenorhabditis elegans Genes. *Genetics*. 210:445-461.

Klaeger, S., S. Heinzlmeir, M. Wilhelm, H. Polzer, B. Vick, P.A. Koenig, M. Reinecke, B. Ruprecht, S. Petzoldt, C. Meng, J. Zecha, K. Reiter, H. Qiao, D. Helm, H. Koch, M. Schoof, G. Canevari, E. Casale, S.R. Depaolini, A. Feuchtinger, Z. Wu, T. Schmidt, L. Rueckert, W. Becker, J. Huenges, A.K. Garz, B.O. Gohlke, D.P. Zolg, G. Kayser, T. Vooder, R. Preissner, H. Hahne, N. Tonisson, K. Kramer, K. Gotze, F. Bassermann, J. Schlegl, H.C. Ehrlich, S. Aiche, A. Walch, P.A. Greif, S. Schneider, E.R. Felder, J. Ruland, G. Medard, I. Jeremias, K. Spiekermann, and B. Kuster. 2017. The target landscape of clinical kinase drugs. *Science*. 358.

Kolch, W., G. Heidecker, G. Kochs, R. Hummel, H. Vahidi, H. Mischak, G. Finkenzeller, D. Marme, and U.R. Rapp. 1993. Protein kinase C alpha activates RAF-1 by direct phosphorylation. *Nature*. 364:249-252.

Lackner, M.R., and S.K. Kim. 1998. Genetic analysis of the Caenorhabditis elegans MAP kinase gene mpk-1. *Genetics*. 150:103-117.

Lackner, M.R., K. Kornfeld, L.M. Miller, H.R. Horvitz, and S.K. Kim. 1994. A MAP kinase homolog, mpk-1, is involved in ras-mediated induction of vulval cell fates in Caenorhabditis elegans. *Genes Dev*. 8:160-173.

Lee, M.H., B. Hook, G. Pan, A.M. Kershner, C. Merritt, G. Seydoux, J.A. Thomson, M. Wickens, and J. Kimble. 2007. Conserved regulation of MAP kinase expression by PUF RNA-binding proteins. *PLoS Genet*. 3:e233.

Ma, J., L. Weng, B.C. Bastian, and X. Chen. 2021. Functional characterization of uveal melanoma oncogenes. *Oncogene*. 40:806-820.

Maziarz, M., A. Leyme, A. Marivin, A. Luebbers, P.P. Patel, Z. Chen, S.R. Sprang, and M. Garcia-Marcos. 2018. Atypical activation of the G protein Gα(q) by the oncogenic mutation Q209P. *J Biol Chem*. 293:19586-19599.

Robinson-Thiewes, S., B. Dufour, P.O. Martel, X. Lechasseur, A.A.D. Brou, V. Roy, Y. Chen, J. Kimble, and P. Narbonne. 2021. Non-autonomous regulation of germline stem cell proliferation by somatic MPK-1/MAPK activity in C. elegans. *Cell Rep*. 35:109162.

Saffer, A.M., D.H. Kim, A. van Oudenaarden, and H.R. Horvitz. 2011. The Caenorhabditis elegans synthetic multivulva genes prevent ras pathway activation by tightly repressing global ectopic expression of lin-3 EGF. *PLoS Genet*. 7:e1002418.

Schadendorf, D., A.C.J. van Akkooi, C. Berking, K.G. Griewank, R. Gutzmer, A. Hauschild, A. Stang, A. Roesch, and S. Ugurel. 2018. Melanoma. *Lancet*. 392:971-984.

Sternberg, P.W., and M. Han. 1998. Genetics of RAS signaling in C. elegans. *Trends Genet*. 14:466-472.

Sundaram, M.V. 2013. Canonical RTK-Ras-ERK signaling and related alternative pathways. *WormBook*:1-38.

Tripathi, R., Z. Liu, A. Jain, A. Lyon, C. Meeks, D. Richards, J. Liu, D. He, C. Wang, M. Nespi, A. Rymar, P. Wang, M. Wilson, and R. Plattner. 2020. Combating acquired resistance to MAPK inhibitors in melanoma by targeting Abl1/2-mediated reactivation of MEK/ERK/MYC signaling. *Nat Commun*. 11:5463.

Turajlic, S., S.J. Furney, G. Stamp, S. Rana, G. Ricken, Y. Oduko, G. Saturno, C. Springer, A. Hayes, M. Gore, J. Larkin, and R. Marais. 2014. Whole-genome sequencing reveals complex mechanisms of intrinsic resistance to BRAF inhibition. *Ann Oncol*. 25:959-967.

Wan, P.T., M.J. Garnett, S.M. Roe, S. Lee, D. Niculescu-Duvaz, V.M. Good, C.M. Jones, C.J. Marshall, C.J. Springer, D. Barford, and R. Marais. 2004. Mechanism of activation of the RAF-ERK signaling pathway by oncogenic mutations of B-RAF. *Cell*. 116:855-867.

Wang, Z., J. Ke, Z. Guo, Y. Wang, K. Lei, S. Wang, G. Chen, Z. Shen, W. Li, and G. Ou. 2024. Transposase-assisted tagmentation: an economical and scalable strategy for single-worm whole-genome sequencing. *G3 (Bethesda)*. 14.

Wooten, D.J., and R. Albert. 2021. synergy: a Python library for calculating, analyzing and visualizing drug combination synergy. *Bioinformatics*. 37:1473-1474.

Wu, Y., M. Han, and K.L. Guan. 1995. MEK-2, a Caenorhabditis elegans MAP kinase kinase, functions in Ras-mediated vulval induction and other developmental events. *Genes Dev*. 9:742-755.

Figure 1

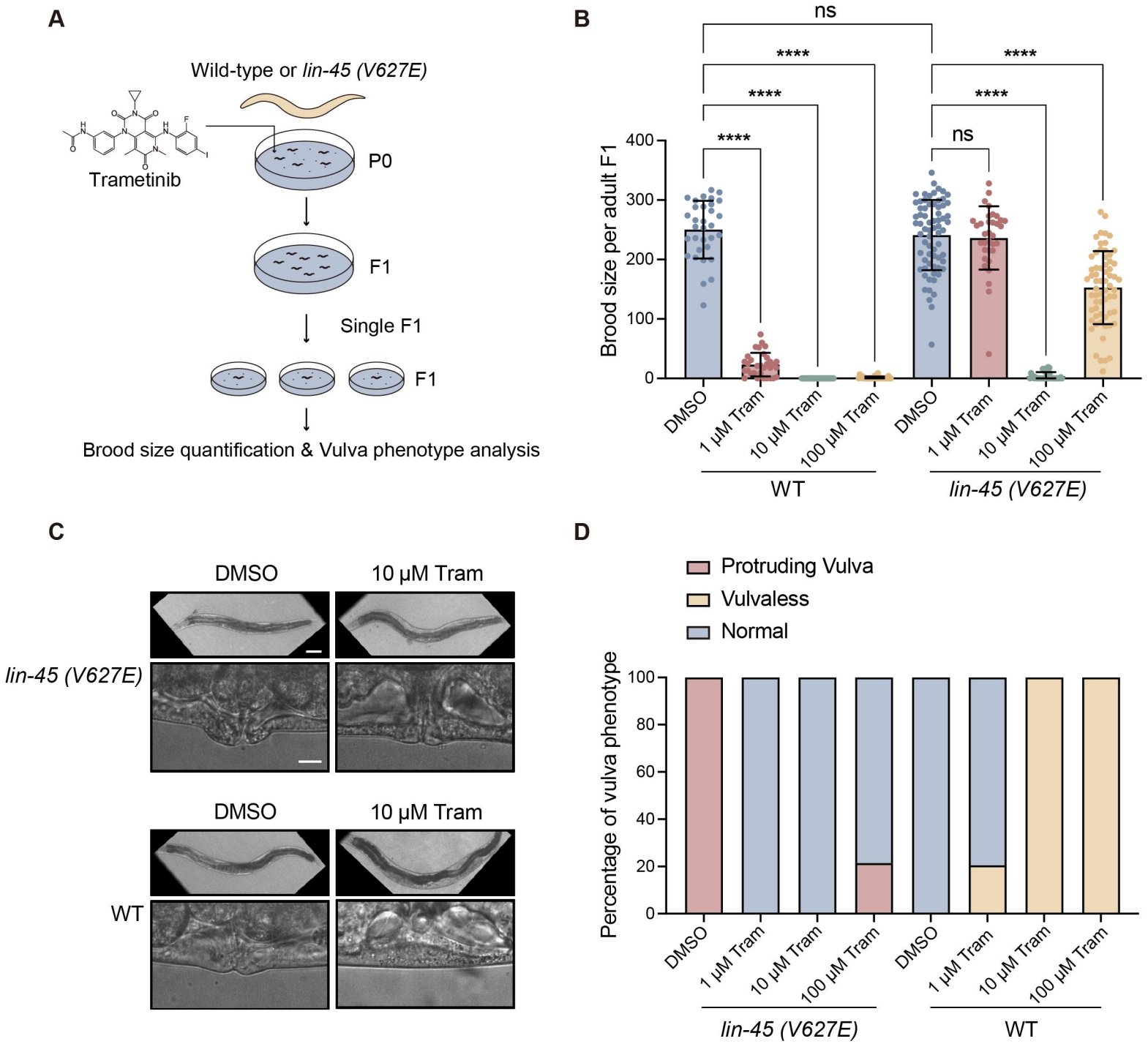
A
Wild-type or lin-45 (V627E)
Trametinib
P0
F1
Single F1
F1
Brood size quantification & Vulva phenotype analysis
B
ns
****
****
****
****
ns
Brood size per adult F1
400
300
200
100
0
DMSO
1 μM Tram
10 μM Tram
100 μM Tram
DMSO
1 μM Tram
10 μM Tram
100 μM Tram
WT
lin-45 (V627E)
C
DMSO
10 μM Tram
lin-45 (V627E)
DMSO
10 μM Tram
WT
D
Protruding Vulva
Vulvaless
Normal
Percentage of vulva phenotype
100
80
60
40
20
0
DMSO
1 μM Tram
10 μM Tram
100 μM Tram
DMSO
1 μM Tram
10 μM Tram
100 μM Tram
lin-45 (V627E)
WT

Figure 1: A *lin-45(V627E) C. elegans* model reveals acquired trametinib resistance under high concentration treatment.

(A) Experimental workflow of brood size quantification and vulva phenotype analysis in wild-type (WT) or *lin-45(V627E)* worms treated with DMSO or different concentrations of trametinib.

(B) Dose-dependent effects of trametinib (Tram) on brood size of WT and *lin-45(V627E)* F1 animals. Mann-Whitney U test and Dunn's multiple comparisons test were used to determine statistical significance. n >35. **** P < 0.0001, ns: not significant.

(C) Representative bright-field images of vulva from *lin-45(V627E)* mutants and wild-type, treated with DMSO and 10 μM trametinib (Tram). n > 35. Scale bar, 10 μm and 100 μm.

(D) Quantification of vulva phenotypes in *lin-45(V627E)* mutants and wild-type (WT) treated with DMSO or different concentrations of trametinib. n >100.

Figure 2

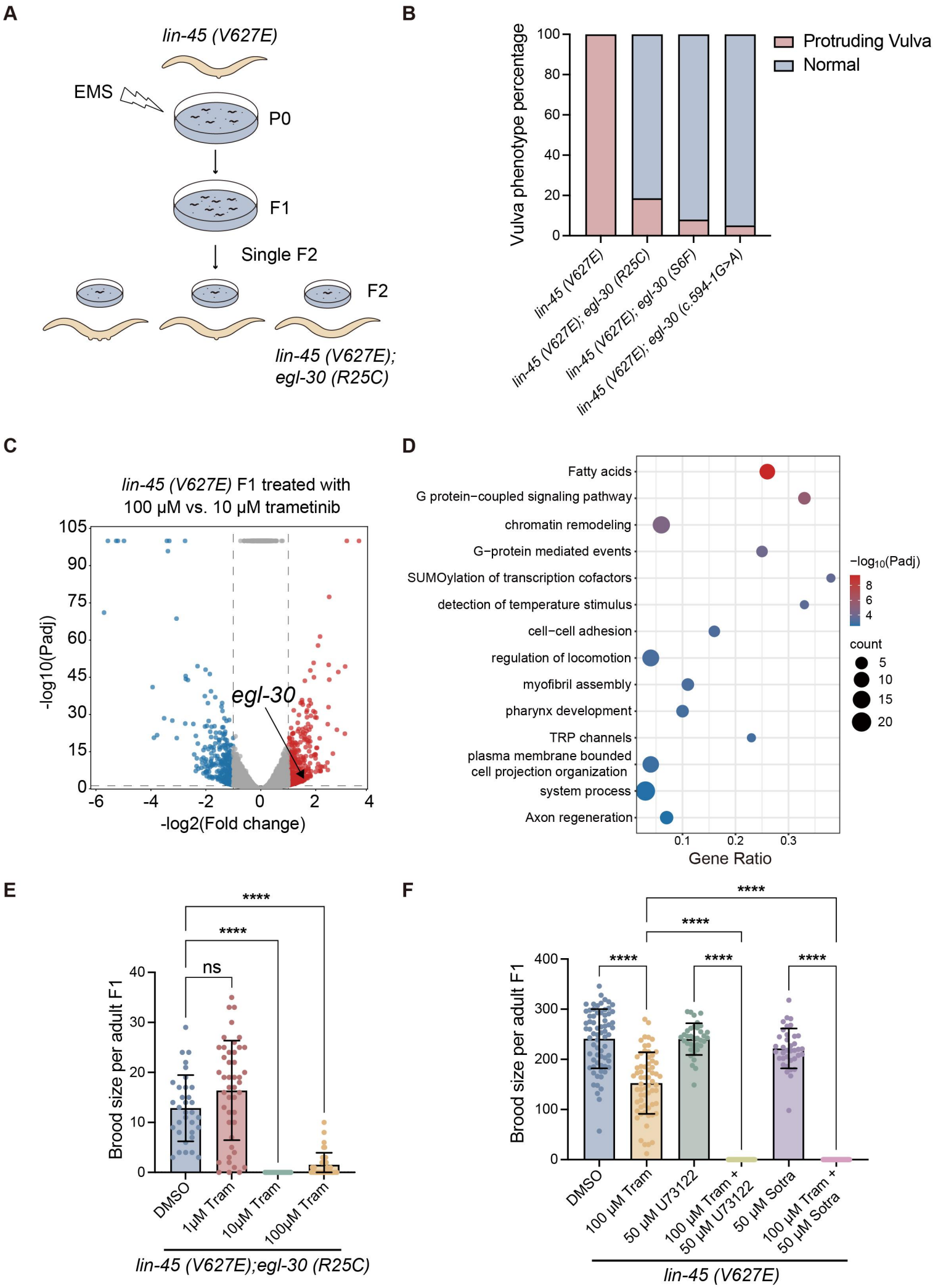
A
lin-45 (V627E)
EMS
P0
F1
Single F2
F2
lin-45 (V627E);
egl-30 (R25C)
B
Vulva phenotype percentage
Protruding Vulva
Normal
lin-45 (V627E)
lin-45 (V627E); egl-30 (R25C)
lin-45 (V627E); egl-30 (S6F)
lin-45 (V627E); egl-30 (c.594-1G>A)
C
lin-45 (V627E) F1 treated with
100 μM vs. 10 μM trametinib
-log10(Padj)
-log2(Fold change)
egl-30
D
Fatty acids
G protein−coupled signaling pathway
chromatin remodeling
G−protein mediated events
SUMOylation of transcription cofactors
detection of temperature stimulus
cell−cell adhesion
regulation of locomotion
myofibril assembly
pharynx development
TRP channels
plasma membrane bounded
cell projection organization
system process
Axon regeneration
Gene Ratio
−log10(Padj)
count
E
Brood size per adult F1
ns
DMSO
1μM Tram
10μM Tram
100μM Tram
lin-45 (V627E);egl-30 (R25C)
F
Brood size per adult F1
DMSO
100 μM Tram
50 μM U73122
100 μM Tram +
50 μM U73122
50 μM Sotra
100 μM Tram +
50 μM Sotra
lin-45 (V627E)

Figure 2: EGL-30/Gαq-PLCβ-PKC signaling is required for acquired trametinib resistance in *lin-45(V627E)* mutants.

(A) Schematic representation of the genetic screening process using EMS mutagenesis on *lin-45(V627E)* worms to identify suppressors exhibiting restored vulval phenotype.

(B) Quantification of vulva phenotypes in *lin-45(V627E)*, *lin-45(V627E); egl-30(R25C), lin-45(V627E); egl-30(S6F)* and *lin-45(V627E); egl-30(c.594-1G>A)* mutants. n >50.

(C) Volcano plot of up- (red) and down-regulated (blue) genes in *lin-45(V627E)* F1 animals treated with 100 μM trametinib compared with those treated with 10 μM trametinib. Fold change > 2 and adjusted P-value (Padj) < 0.05. n = 3 biological replicates per treatment.

(D) Dot plot of gene ontology (GO) enrichment of the up-regulated genes in the *lin-45(V627E)* F1 animals treated with 100 μM trametinib.

(E) Dose-dependent effects of trametinib (Tram) on brood size of *lin-45(V627E); egl-30(R25C)* F1 animals. Dunn's multiple comparisons test were used to determine statistical significance. n >35. **** P < 0.0001, ns: not significant.

(F) Brood sizes of WT and *lin-45(V627E)* F1 animals treated with DMSO, 50 μM U73122, 50 μM sotrastaurin (Sotra), 100 μM trametinib (Tram), or the combination. Dunn's multiple comparisons test was used to determine statistical significance. n >35. **** P < 0.0001.

Figure 3

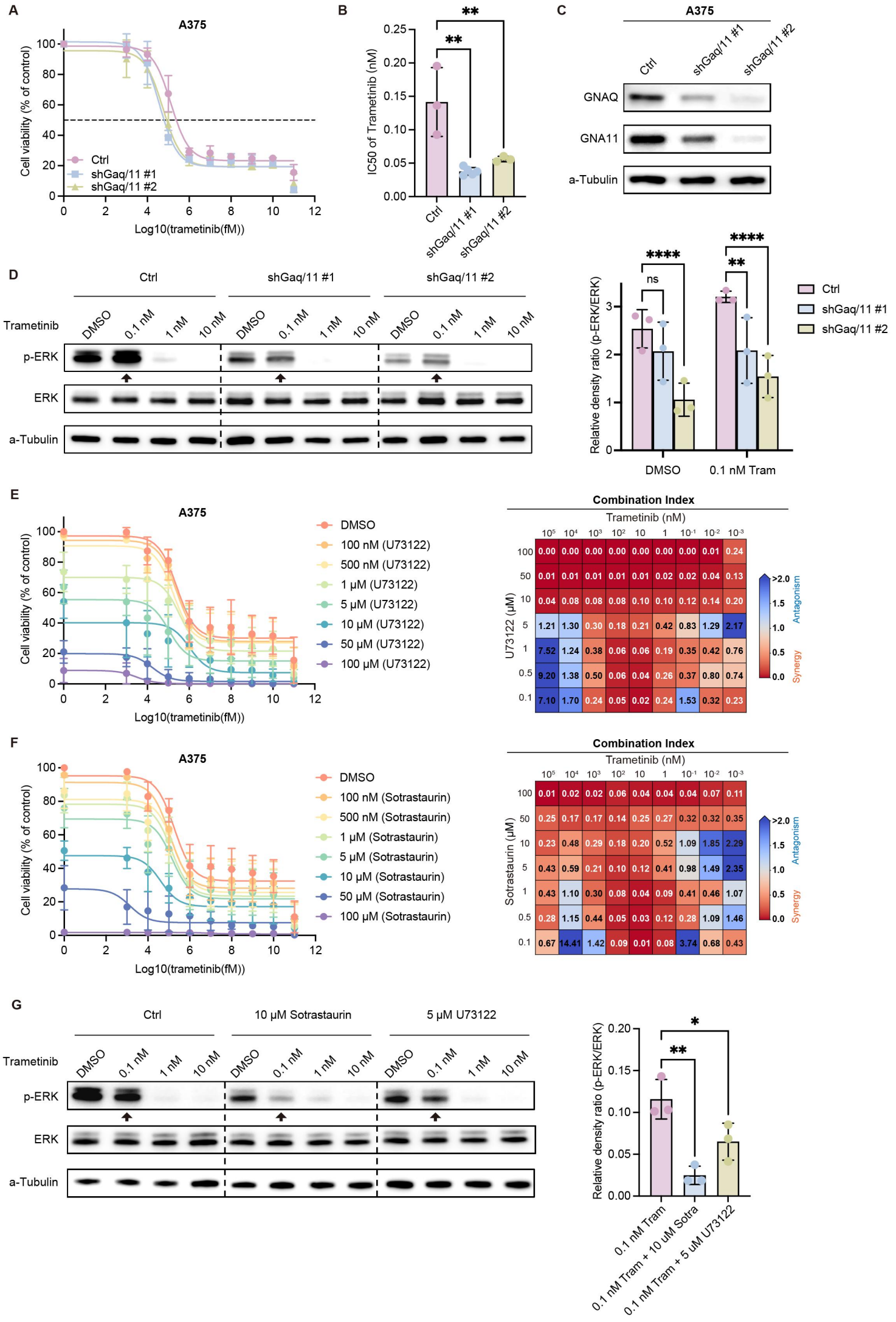
A
A375
Cell viability (% of control)
Log10(trametinib(fM))
Ctrl
shGaq/11 #1
shGaq/11 #2
B
IC50 of Trametinib (nM)
Ctrl
shGaq/11 #1
shGaq/11 #2
C
A375
Ctrl
shGaq/11 #1
shGaq/11 #2
GNAQ
GNA11
a-Tubulin
D
Ctrl
shGaq/11 #1
shGaq/11 #2
Trametinib
DMSO
0.1 nM
1 nM
10 nM
p-ERK
ERK
a-Tubulin
Relative density ratio (p-ERK/ERK)
ns
DMSO
0.1 nM Tram
E
A375
Cell viability (% of control)
Log10(trametinib(fM))
DMSO
100 nM (U73122)
500 nM (U73122)
1 μM (U73122)
5 μM (U73122)
10 μM (U73122)
50 μM (U73122)
100 μM (U73122)
Combination Index
Trametinib (nM)
U73122 (μM)
Antagonism
Synergy
F
A375
Cell viability (% of control)
Log10(trametinib(fM))
DMSO
100 nM (Sotrastaurin)
500 nM (Sotrastaurin)
1 μM (Sotrastaurin)
5 μM (Sotrastaurin)
10 μM (Sotrastaurin)
50 μM (Sotrastaurin)
100 μM (Sotrastaurin)
Combination Index
Trametinib (nM)
Sotrastaurin (μM)
Antagonism
Synergy
G
Ctrl
10 μM Sotrastaurin
5 μM U73122
Trametinib
DMSO
0.1 nM
1 nM
10 nM
p-ERK
ERK
a-Tubulin
Relative density ratio (p-ERK/ERK)
0.1 nM Tram
0.1 nM Tram + 10 uM Sotra
0.1 nM Tram + 5 uM U73122

Figure 3. Synergistic inhibition of A375 cell proliferation by Gαq/11–PLCβ–PKC blockade and MEK inhibition.

(A) A375 cells transduced with empty vector control (Ctrl) or shRNA targeting both GNAQ and GNA11 (shGαq/11) were treated with vehicle or trametinib for 72 h. Cell viability was measured by CellTiter-Glo, and dose-response curves are shown (mean ± SD, n = 3 independent experiments).

(B) IC_{50} values of trametinib in A375 cells transduced with Ctrl or shGαq/11. n = 3, ** $P < 0.01$.

(C) Knockdown efficiency of A375 cells transduced with shGαq/11 was verified by western blot.

(D) Western blot analysis of indicated proteins in A375 cells transduced with Ctrl or shGαq/11 treated with DMSO or trametinib at the indicated concentrations for 24 h. A representative blot (left) (n = 3 independent experiments) and quantification of pERK (right) are shown, ** $P < 0.01$, **** $P < 0.0001$, ns: not significant.

(E) Dose-response curves of viability (left) and Chou-Talalay combination index (CI) diagram (right) of A375 cells treated with U73122 in combination with trametinib at the indicated concentrations for 72 h (mean ± SD, n = 3). CI < 0.3, strong synergy (red); 0.3-0.9, synergy; 0.90-1.1, additive; ≥ 1.1, antagonism (blue).

(F) Dose-response curves of viability (left) and CI diagram (right) of A375 cells treated with sotrastaurin (Sotra) in combination with trametinib at the indicated concentrations for 72 h (mean ± SD, n = 3).

(G) Western blot analysis of indicated proteins in A375 cells treated with DMSO, or 10 μM sotrastaurin (Sotra) or 5 μM U73122, alone or with trametinib at the indicated concentrations for 24 h. A representative blot (left) (n = 3 independent experiments) and quantification of pERK (right) are shown, * $P < 0.1$, ** $P < 0.01$.

Figure 4

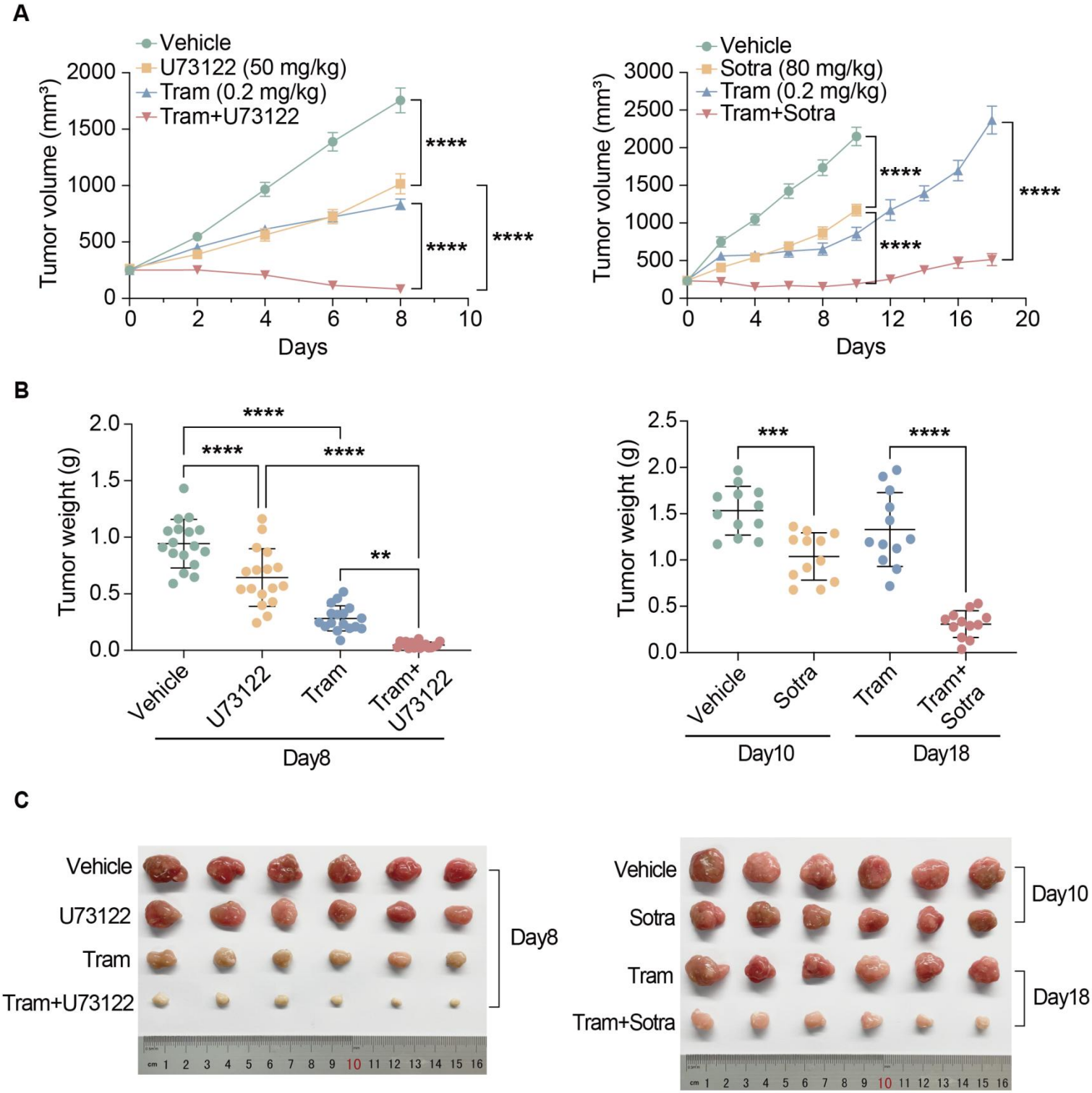
A
Vehicle
U73122 (50 mg/kg)
Tram (0.2 mg/kg)
Tram+U73122
Tumor volume (mm³)
Days
****
Vehicle
Sotra (80 mg/kg)
Tram (0.2 mg/kg)
Tram+Sotra
B
Tumor weight (g)
Vehicle
U73122
Tram
Tram+ U73122
Day8
**
***
Sotra
Tram+ Sotra
Day10
Day18
C
Vehicle
U73122
Tram
Tram+U73122
Sotra
Tram+Sotra
Day8
Day10
Day18

Figure 4. Combined PLCβ-PKC and MEK inhibition synergistically suppresses tumor growth.

(A) Tumor volumes of mice measured at different time points after treatment. Mice bearing parental A375 xenografts were randomized into four groups (n = 12/group) and treated with vehicle, 50 mg/kg U73122, 80 mg/kg sotrastaurin (Sotra), 0.2 mg/kg trametinib (Tram), or the indicated combinations when average tumor size reached 250 mm^3. Data represent mean ± SEM; some error bars are too small to be visible. Statistical significance was determined by two-way ANOVA followed by Tukey's multiple comparisons test. **** $P < 0.0001$.

(B) Tumor weights at the end of treatment. Mice treated with vehicle, U73122, Sotra, Tram, or the indicated combinations were euthanized on days 8, 10, or 18 as indicated, and tumors were removed and weighed. Statistical significance was determined by one-way ANOVA followed by Tukey's multiple comparisons test. ** $P < 0.01$, *** $P < 0.001$, **** $P < 0.0001$.

(C) Representative tumor photographs from each treatment group collected at the end of treatment.

Figure 5

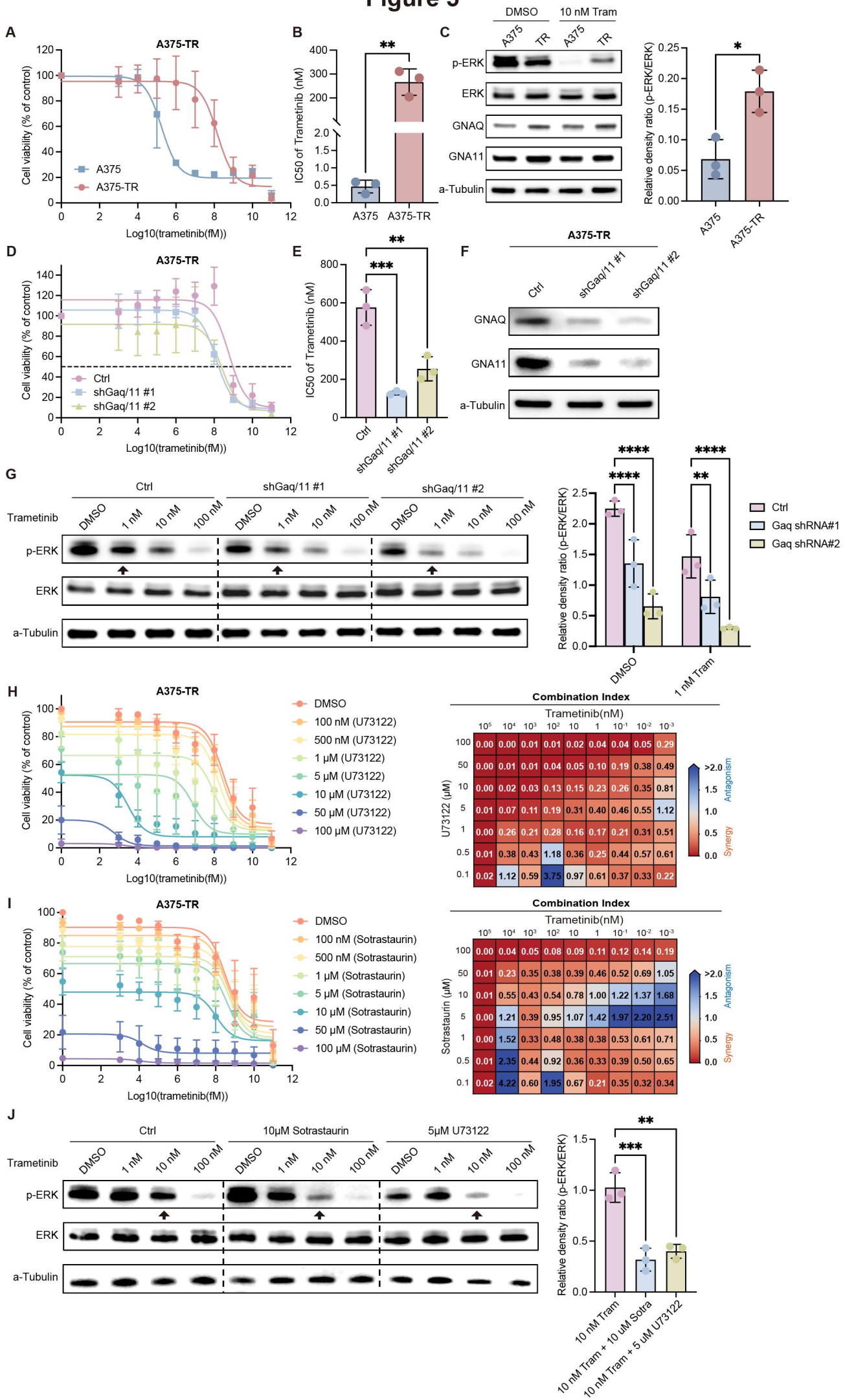
A
A375-TR
Cell viability (% of control)
Log10(trametinib(fM))
A375
A375-TR
B
IC50 of Trametinib (nM)
A375
A375-TR
C
DMSO
10 nM Tram
A375
TR
A375
TR
p-ERK
ERK
GNAQ
GNA11
a-Tubulin
Relative density ratio (p-ERK/ERK)
A375
A375-TR
D
A375-TR
Cell viability (% of control)
Log10(trametinib(fM))
Ctrl
shGaq/11 #1
shGaq/11 #2
E
IC50 of Trametinib (nM)
Ctrl
shGaq/11 #1
shGaq/11 #2
F
A375-TR
Ctrl
shGaq/11 #1
shGaq/11 #2
GNAQ
GNA11
a-Tubulin
G
Ctrl
shGaq/11 #1
shGaq/11 #2
Trametinib
DMSO
1 nM
10 nM
100 nM
p-ERK
ERK
a-Tubulin
Relative density ratio (p-ERK/ERK)
DMSO
1 nM Tram
Ctrl
Gaq shRNA#1
Gaq shRNA#2
H
A375-TR
Cell viability (% of control)
Log10(trametinib(fM))
DMSO
100 nM (U73122)
500 nM (U73122)
1 μM (U73122)
5 μM (U73122)
10 μM (U73122)
50 μM (U73122)
100 μM (U73122)
Combination Index
Trametinib(nM)
U73122 (μM)
Antagonism
Synergy
I
A375-TR
Cell viability (% of control)
Log10(trametinib(fM))
DMSO
100 nM (Sotrastaurin)
500 nM (Sotrastaurin)
1 μM (Sotrastaurin)
5 μM (Sotrastaurin)
10 μM (Sotrastaurin)
50 μM (Sotrastaurin)
100 μM (Sotrastaurin)
Combination Index
Trametinib(nM)
Sotrastaurin (μM)
Antagonism
Synergy
J
Ctrl
10μM Sotrastaurin
5μM U73122
Trametinib
DMSO
1 nM
10 nM
100 nM
p-ERK
ERK
a-Tubulin
Relative density ratio (p-ERK/ERK)
10 nM Tram
10 nM Tram + 10 uM Sotra
10 nM Tram + 5 uM U73122

Figure 5. Synergistic inhibition of trametinib-resistant A375 (A375-TR) cell proliferation by Gαq/11–PLCβ–PKC blockade and MEK inhibition.

(A) Parental A375 and A375-TR cells were treated with vehicle or trametinib for 72 h. Cell viability was measured by CellTiter-Glo, and dose-response curves are shown (mean ± SD, n = 3 independent experiments).

(B) IC_{50} values of trametinib in A375 and A375-TR cells. n = 3, ** P < 0.01.

(C) Western blot analysis of indicated proteins in A375 and A375-TR cells treated with DMSO or trametinib at the indicated concentrations for 24 h. A representative blot (left) (n = 3 independent experiments) and quantification of pERK (right) are shown, * P < 0.1.

(D) A375-TR cells transduced with empty vector control (Ctrl) or shRNA targeting both GNAQ and GNA11 (shGαq/11) were treated with vehicle or trametinib for 72 h. Cell viability was measured by CellTiter-Glo, and dose-response curves are shown (mean ± SD, n = 3 independent experiments).

(E) IC_{50} values of trametinib in A375-TR cells transduced with Ctrl or shGαq/11. n = 3, **p < 0.01, *** P < 0.001.

(F) Knockdown efficiency of A375-TR cells transduced with shGαq/11 was verified by western blot.

(G) Western blot analysis of indicated proteins in A375-TR cells transduced with Ctrl or shGαq/11 treated with DMSO or trametinib at the indicated concentrations for 24 h. A representative blot (left) (n = 3 independent experiments) and quantification of pERK (right) are shown, ** P < 0.01, **** P < 0.0001.

(H) Dose-response curves of viability (left) and Chou-Talalay combination index (CI) diagram (right) of A375-TR cells treated with U73122 in combination with trametinib at the indicated concentrations for 72 h (mean ± SD, n = 3). CI < 0.3, strong synergy (red); 0.3-0.9, synergy; 0.90-1.1, additive; ≥ 1.1, antagonism (blue).

(I) Dose-response curves of viability (left) and CI diagram (right) of A375-TR cells treated with sotrastaurin (Sotra) in combination with trametinib at the indicated concentrations for 72 h (mean ± SD, n = 3).

(J) Western blot analysis of indicated proteins in A375-TR cells treated with DMSO, 10 μM sotrastaurin (Sotra) or 5 μM U73122, alone or with trametinib at the indicated concentrations for 24 h. A representative blot (left) (n = 3 independent experiments) and quantification of pERK (right) are shown, ** P < 0.01, *** P < 0.001.

Figure S1

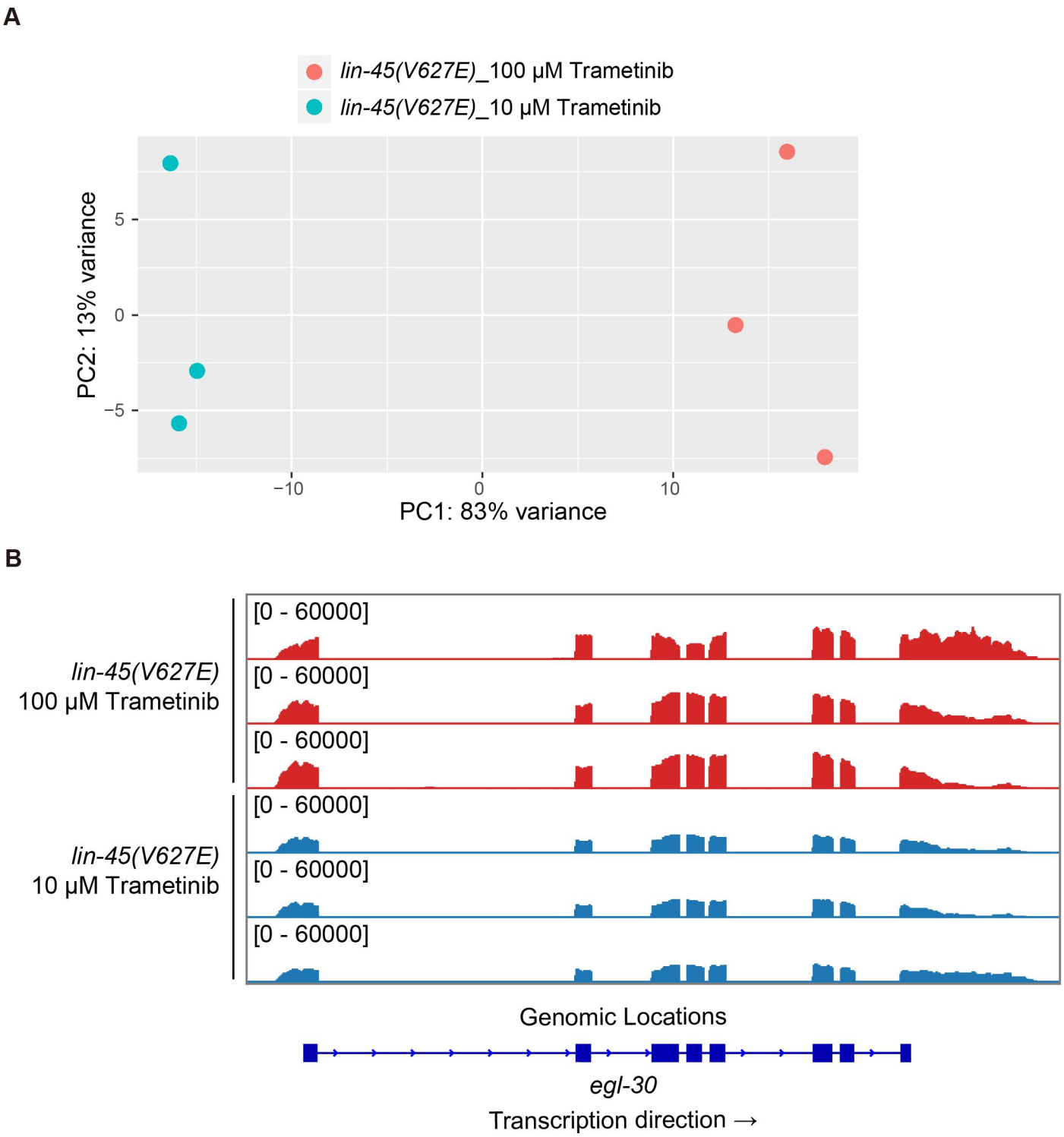

Figure S1. EGL-30/Gαq is upregulated in *lin-45(V627E)* mutant resistant to trametinib.

(A) Principal component analysis (PCA) of RNA-seq data from *lin-45(V627E)* F1 animals treated with 100 µM or 10 µM trametinib (n = 3 biological replicates per condition).

(B) Integrative Genomics Viewer (IGV) visualization showing normalized RNA-seq read distributions at the *egl-30* locus in *lin-45(V627E)* F1 animals treated with 100 µM or 10 µM trametinib.

Figure S2

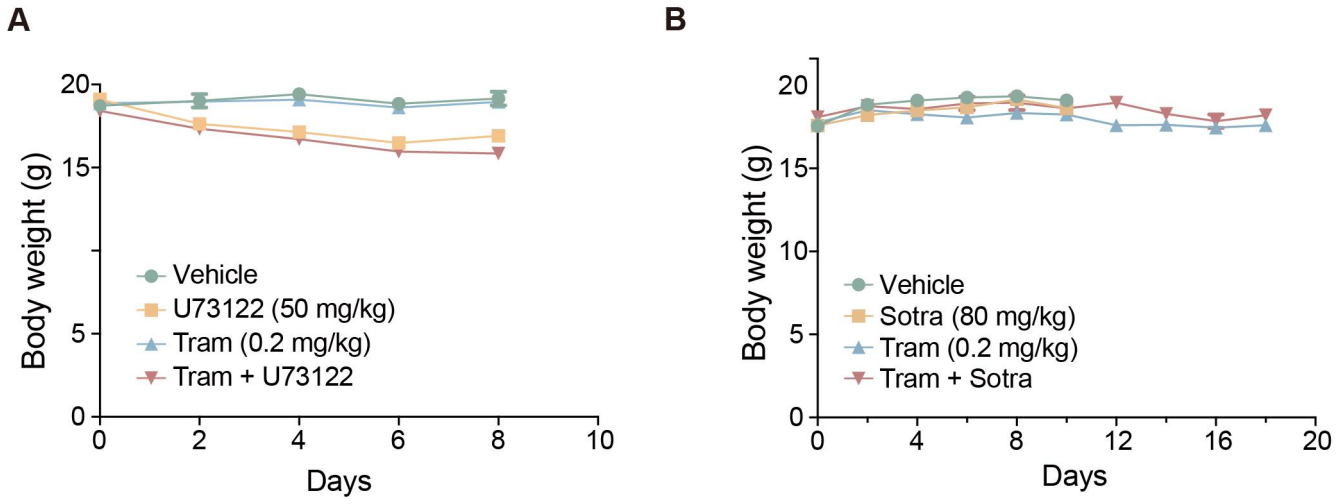

Figure S2. Body weight of A375 xenograft-bearing mice under different treatments.

(**A-B)** Body weight of mice measured at different time points after treatment. Mice bearing parental A375 xenografts were randomized into four groups (n = 12/group), and treated with vehicle, 50 mg/kg U73122, 80 mg/kg sotrastaurin (Sotra), 0.2 mg/kg trametinib or the combination when average tumor size reached 250 mm^3. Data represent mean ± SEM.